Supporting Information

A MOF Platform for Incorporation of Complementary Organic Motifs for CO_2 Binding

Pravas Deria,[a] Song Li,[b] Hongda Zhang,[b] Randall Q. Snurr,[b] Joseph T. Hupp,*[a] and Omar K. Farha*[a,c]*

[a] Department of Chemistry, Northwestern University, 2145 Sheridan Road, Evanston, Illinois 60208, United States
[b] Department of Chemical and Biological Engineering, Northwestern University, 2145 Sheridan Road, Evanston, Illinois 60208, United States
[c] Department of Chemistry, Faculty of Science, King Abdulaziz University, Jeddah, Saudi Arabia

Table of Contents

S1. Materials

Solvents, acetone, *N,N*-dimethylformamide (DMF), ethyl acetate, diethyl ether, chloroform, and dichloromethane were purchased from Macron; deuterated dimethyl sulfoxide (d_6-DMSO) (Cambridge Isotopes, 99%), and deuterated sulfuric acid (Cambridge Isotopes, 96-98% solution in D_2O) were used as received without further purification. The N-α-fluorenylmethyloxycarbonyl protected tripeptide, Fmoc-glycyl-glycyl-glycine (or Fmoc-Gly-Gly-Gly-OH), **F3G-H** was purchased from Chem-Impex International Inc., USA and was used as received. 2,6-Dibromopyridine-1-oxide, NH_4OH (28% in water), acetyl bromide (sure seal), benzylamine (sure seal), acetic acid, acetic anhydride, pyridine, *N*-formylsaccharin, Xantphos, palladium(II)acetate, anhydrous potassiumfluoride, and anhydrous DMF were purchased from Aldrich and used as received. H_4TBAPy [1,3,6,8-tetrakis(p-benzoic-acid)pyrene][1] was synthesized according to previous procedure.[2] Pristine microcrystalline **NU-1000**[2] was obtained after treating the as-synthesized material (~50 mg) (including removal of ligated and free benzoate/benzoic acid) with 0.5 mL of 8 M HCl (aq) in DMF (12 mL) at elevated temperature (100 ºC),[2-4] followed by washing with fresh solvents (DMF + acetone) and finally drying under vacuum (~100 torr) for 30 min at 50 °C.

S2. Instrumentation

Standard Schlenk techniques were employed to manipulate air-sensitive syntheses; which were carried out under nitrogen previously passed through an O_2 scrubbing tower (GetterMax 133 catalyst, Research Catalysts, Inc) and a drying tower (Linde 3-Å molecular sieves). ^{1}H NMR spectra were collected on an Agilent 400 MHz instrument; for the SALI-derived materials the spectra were recorded after digesting the samples in 10% D_2SO_4/DMSO-d_6 and were referenced to the residual solvent peak; ^{13}C NMR spectra were collected on a Bruker 500 MHz instrument. Powder X-ray diffraction (PXRD) patterns were recorded on a Rigaku ATXG diffractometer equipped with an 18 kW Cu rotating anode, MLO monochromator, and a high-count-rate scintillation detector (in 0.05° step width with a 2 deg/min scanning speed). Diffuse reflectance infrared spectra (DRIFTS) were recorded on a Nicolet 7600 FTIR spectrometer equipped with an MCT detector. The spectra were collected in a KBr mixture under N_2 purge using KBr as the background. Nitrogen isotherms were measured on a Micromeritics TriStar II 3020 at 77 K; for BET surface area analyses, the two consistency criteria described by Rouquerol et al.[5] [6] were satisfied. Pore size distribution was calculated using Barrett-Joyner-Halenda (BJH) method with Halsey thickness curve and Kruk-Jaroniec-Sayari correction applied.[7] Multi-temperature CO_2 and N_2 adsorption isotherms were collected on a Hiden Isochema Intelligent Gravimetric Analyzer (IGA-200), equipped with a micro-gram balance; all CO_2 isotherms were recorded using IGASwin software (v.1) that utilizes a linear driving force model (@ >96% equilibration had been reached) and corrects all data points for the buoyancy effects; thus the adsorbed mass at a given pressure was the difference of mass gain at that point relative to the evacuated sorbent mass recorded at $P = 10^{-7}$ torr.

S3. Synthesis and Characterization of **DAP-H** and **SALI-**derived Materials

S3A. Synthesis of DAP-H

2,6-Di(acylamino)-4-bromopyridine (**F**)[8] was prepared following Scheme SI-1 from 2,6-dibromopyridine-1-oxide as a precursor according to literature procedure.[9]

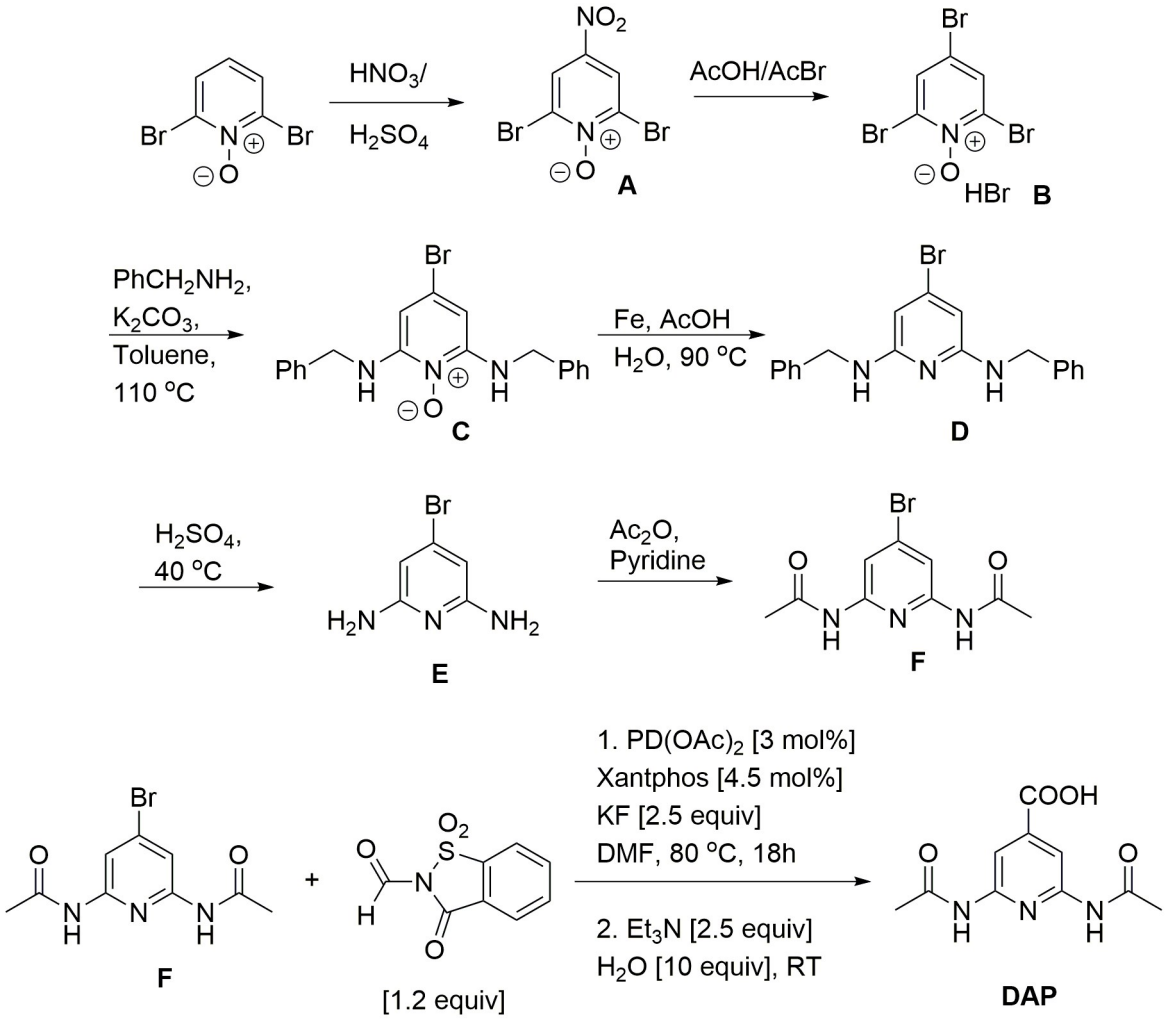

Scheme SI-1. Synthesis of 2,6-di(acylamino)-4-carboxypyridine (**DAP**).

2,6-Dibromo-4-nitropyridine-1-oxide (A).[9] 2,6-Dibromopyridine-*N*-oxide (10 g; 39.5 mmol) was added to a mixture of concentrated sulfuric acid (33 mL) and fuming nitric acid (14 mL) and the mixture was stirred at 60 °C for 22 h. The reaction mixture was cooled to room temperature and quenched with ice cold NH_4OH (28% in H_2O). The yellowish white precipitate was filtered, washed with cold water, and air dried to yield 10.2 g (34.3 mmol; 87%) of product A. ^1H NMR (400 MHz, $CDCl_3$ as 7.26 ppm): δ 8.50 (s).

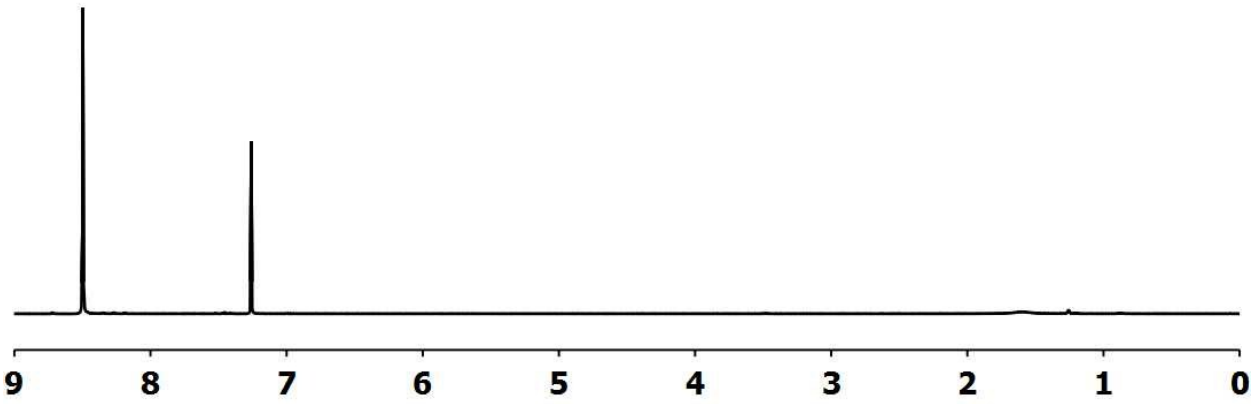

Figure SI-1A. ^{1}H NMR spectrum of 2,6-dibromo-4-nitropyridine-*N*-oxide (**A**) recorded in $CDCl_3$.

2,4,6-Tribromopyridine-1-oxide hydrobromide (B).[9] To a slurry of compound **A** (25 g; 83.9 mmol) in acetic acid (415 mL) acetyl bromide (6.3 mL; 84.7 mmol) was added under stirring at 60 °C. The temperature was raised to 80 °C and stirred for another 6h. The reaction mixture was then cooled to room temperature and further with ice bath. The precipitate was filtered, washed with ~100 mL of diethyl ether, and air dried to obtain 23 g (55.7 mmol; 66%) of product **B** as a white solid. ^{1}H NMR (400 MHz, dmso-d_6 as 2.50 ppm): δ 8.31 (s).

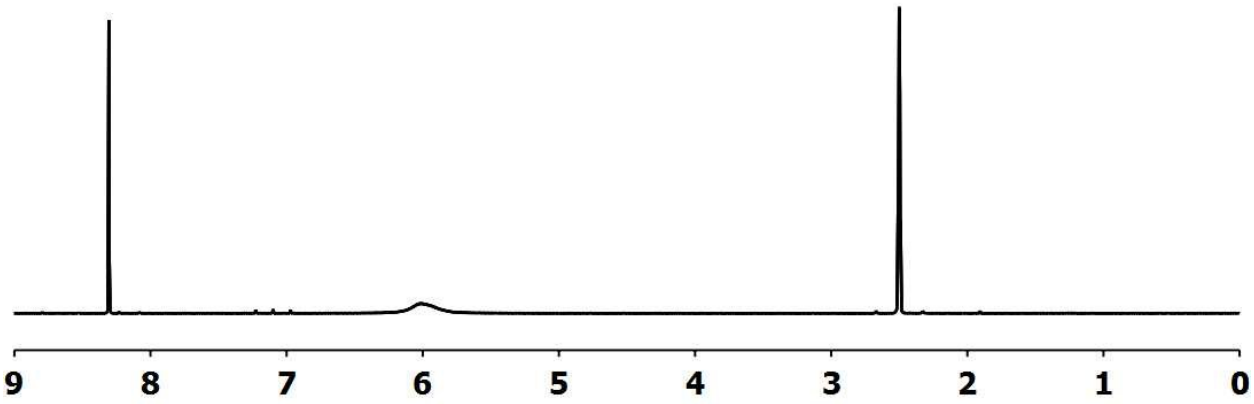

Figure SI-1B. ^{1}H NMR spectrum of 2,4,6-tribromopyridine-*N*-oxide (**B**) recorded in dmso-d_6.

***N,N'*-Dibenzyl-4-bromo-1-oxypyridine-2,6-diamine (C)**.[9] Anhydrous K_2CO_3 (26 g; 188.40 mmol) and anhydrous toluene (350 mL) were taken in a 500 mL round bottomed flask under nitrogen atmosphere. Compound B (23 g; 55.70 mmol) was added to the reaction mixture. Benzylamine (60 g; 560.00 mmol) was added slowly via syringe and the reaction mixture was stirred under nitrogen at 110 °C for 24 h. After cooling, the reaction was washed with brine and the organic layer was evaporated to dryness under reduced pressure. The dark solid was dissolved in dichloromethane (~75 mL) and the product was crystallized following trituration with hexane (~100 mL) to yield 18 g (46.9 mmol; 84%) of product **C** as beige colored crystalline solid. ^{1}H NMR (400 MHz, $CDCl_3$ as 7.26 ppm): δ 7.38-7.28 (m; 10H, Ph), 7.17 (t, J = 6.0 Hz, 2H, NH), 6.03 (s, 2H, Py), 4.45 (d, J = 6.0 Hz, 4H, CH_2Ph).

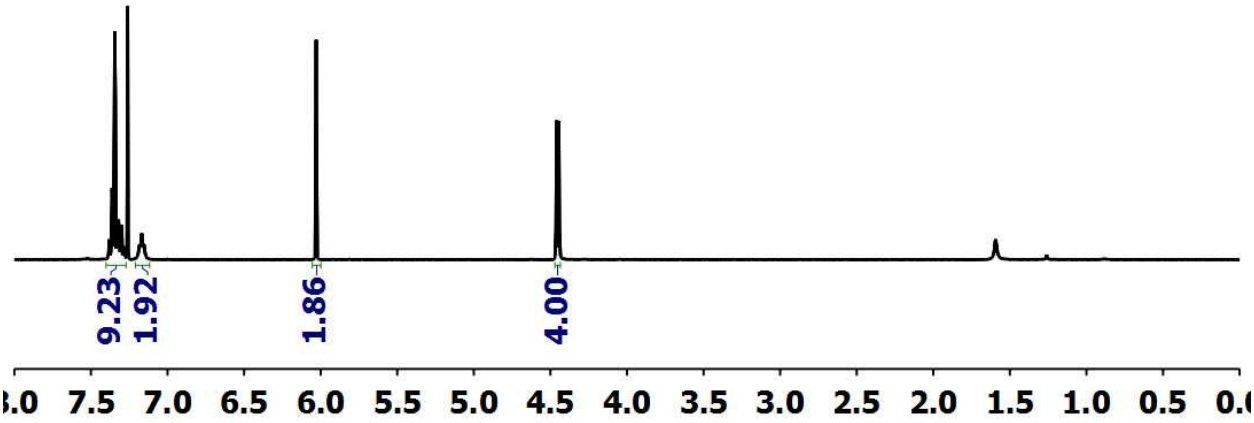

Figure SI-1C. ^{1}H NMR spectrum of *N,N'*-dibenzyl-4-bromo-1-oxypyridine-2,6-diamine (**C**) recorded in $CDCl_3$.

***N,N'*-Dibenzyl-4-bromopyridine-2,6-diamine (D)**.[9] Iron powder (3.5 g; 66.67 mmol) was added slowly at once to a slurry of compound C (16 g; 41.67mmol) in 1:1 solvent mixture of acetic acid and water (200 mL). The reaction mixture was stirred at 90 °C for 4 h and then cooled to room temperature. The reaction mixture was then diluted with ethyl acetate and neutralized with 30% NaOH solution under magnetic stirring and then filtered through ~ 100 g silica. The silica was washed with ethyl acetate (50×2 mL) and the total filtrate was separated. The organic layer was washed with water (150×2 mL) and evaporated to dryness. The dark solid was dissolved in dichloromethane (30 mL), filtered through silica (100 g) with dichloromethane. The solution was evaporated to yield 14 g (38.1 mmol; 92%) of product **D** as beige colored solid. ^{1}H NMR (400 MHz, $CDCl_3$ as 7.26 ppm): δ 7.36-7.25 (m; 10H, Ph), 5.92 (s, 2H, Py), 4.67 (t, J = 5.6 Hz, 2H, NH), 4.43 (d, J = 6.0 Hz, 4H, CH_2Ph).

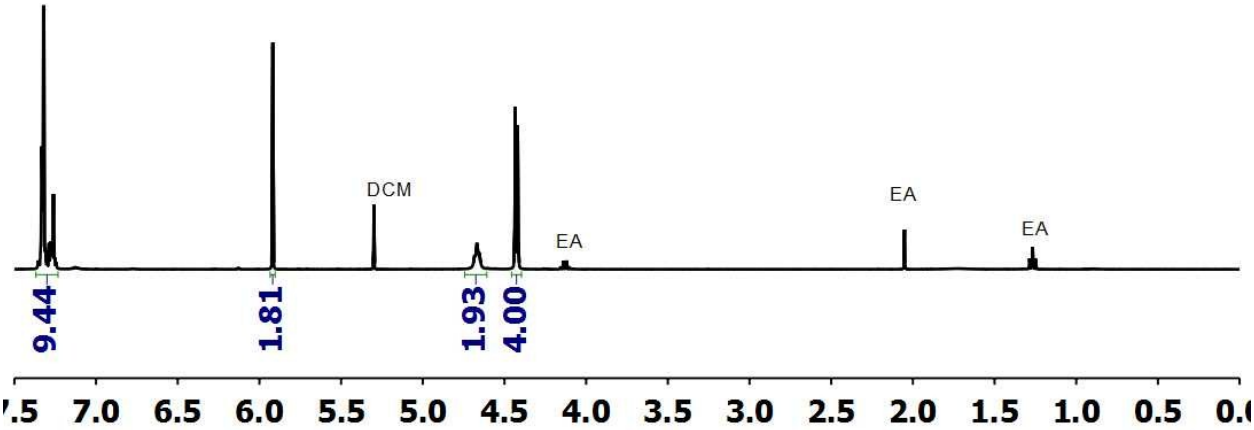

Figure SI-1D. ^{1}H NMR spectrum of *N,N'*-dibenzyl-4-bromopyridine-2,6-diamine (**D**) recorded in $CDCl_3$. (Peaks for residual ethyl acetate (EA) and dichloromethane are marked accordingly).

4-Bromopyridine-2,6-diamine (E).[9] Concentrated sulfuric acid (70 mL) was taken in a 200 mL round bottomed flask, compound D (14 g; 38.10 mmol) was slowly added to it. The reaction mixture was warmed to 40 °C and stirred for 2 h. The reaction mixture was then slowly poured into 400 g of crushed ice and neutralized with NH_4OH (30%). This mixture was taken into a separatory funnel and the extracted twice with ethyl acetate. After washing with water (300×2 mL), the organic layer was dried. The solid residue was dissolved and filtered with ethyl acetate over ~75 g of silica. The organic layer was finally dried to yield 4.4 g (23.5 mmol; 62%) of

product **E** as beige colored crystalline solid. ^{1}H NMR (400 MHz, $CDCl_3$ as 7.26 ppm): δ 6.05 (s, 2H, Py), 4.24 (s, *br*, 4H, NH_2).

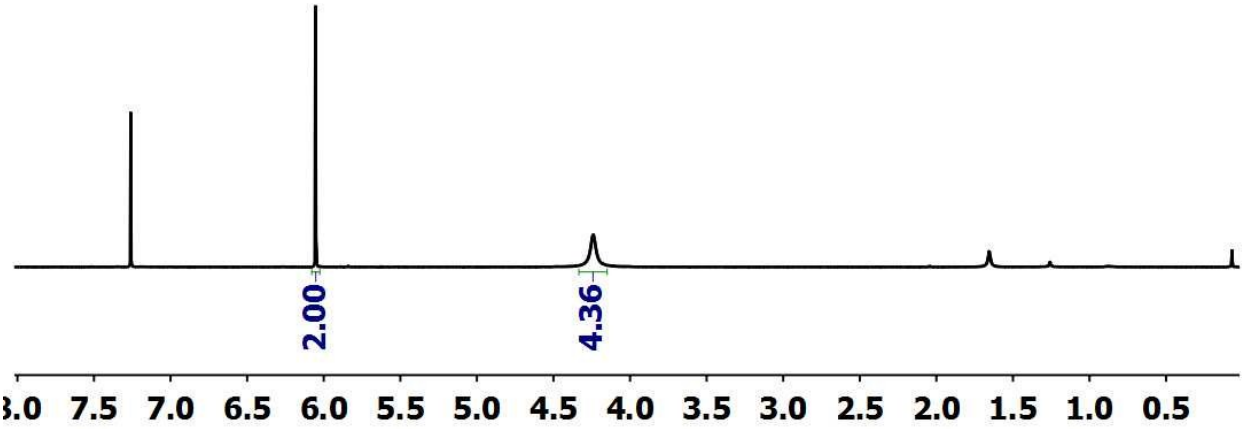

Figure SI-1E. ^{1}H NMR spectrum of 4-bromopyridine-2,6-diamine (**E**) recorded in $CDCl_3$.

2,6-Di(acylamino)-4-bromopyridine (F).[8] Compound E (4.4 g; 23.5 mmol) was taken in a 100 mL reaction tube and dissolved in pyridine (15 mL). A 25 mL portion of acetic anhydride (264 mmol) was then slowly added to the reaction mixture. The reaction mixture was stirred at room temperature for 24 h and then diluted with chloroform (100 mL), which was washed with brine. The organic layer was dried over anhydrous sodium sulfate and concentrated under reduced pressure. The product was precipitated via trituration with diethyl ether (~20 mL) to yield 4.7 g (17.6 mmol; 75%) of product **F** as pale yellow white solid. ^{1}H NMR (400 MHz, CD_3OD as 3.34 ppm): δ 8.04 (s, 2H, Py), 4.88 (s, 2H, NH), 2.19 (s, CH_3).

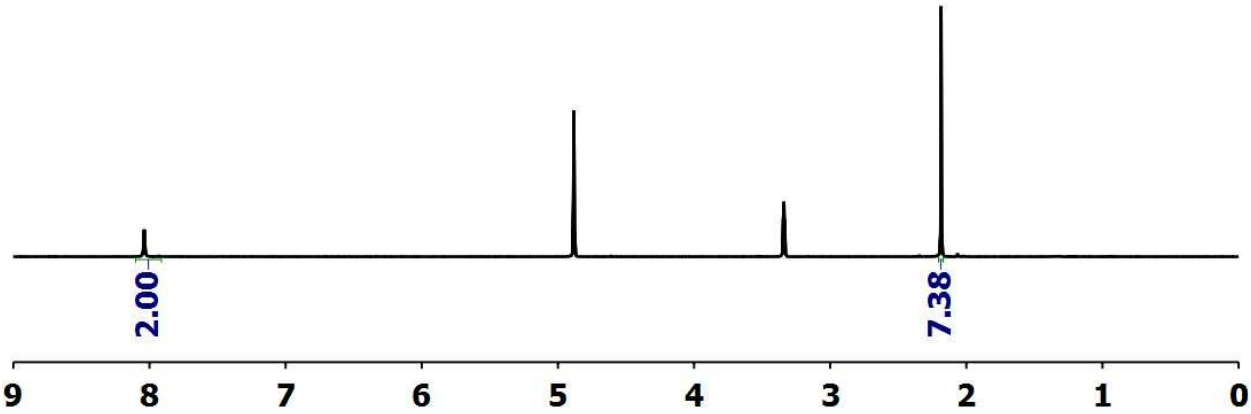

Figure SI-1F. ^{1}H NMR spectrum of 2,6-di(acylamino)-4-bromopyridine- (**F**) recorded in CD_3OD.

2,6-Di(acylamino)-4-carboxypyridine (DAP-H).[10] 2,6-Di(acylamino)-4-bromopyridine (630.0 mg, 2.32 mmol, 1 equiv), $Pd(OAc)_2$ (15.0 mg, 0.07 mmol, 3.0 mol %), xantphos (60.0 mg, 0.104 mmol, 4.5 mol %), N-formylsaccharin (590.0 mg, 2.8 mmol, 1.2 equiv), and KF (336 mg, 5.8 mmol, 2.5 equiv) were taken in a 50 mL Schlenk tube and was charged with N_2. Then, a degassed DMF (15 mL, via bubbling N_2 for 1h) was transferred to the reaction tube via cannula and then stirred at 80 °C for 18 h. The reaction mixture (crimson colored slurry) was cooled to room temperature. A 810 µL portion of Et_3N (5.8 mmol, 2.5 equiv) followed by a 420 µL of water (23.2 mmol, 10 equiv) was added to the reaction mixture, which was stirred at room

temperature for 3 h, following which the solvent was evaporated under reduced pressure. The solid was washed with water to remove the saccharin and other salts and then air dried on top of a fine glass frit. The pale white solid was dissolved in methanol-acetonitrile mixture (1:2, ~10 mL) and precipitated by slow addition of ether; this precipitation was carried out 3 times to get the DAP product as a white solid. Yield = 450 mg (83%, based on 630 mg 2,6-di(acylamino)-4-bromopyridine). ^{1}H NMR (400 MHz, dmso-d_6 as 2.5 ppm, Figure SI-1): δ 13.50 (br-s, 1H), 10.264 (s, 2H), 8.198 (s, 2H), 2.124 (s, 6H). ^{13}C NMR (125 MHz, dmso-d_6 as 39.52 ppm): δ 169.546, 166.134, 151.102, 141.919, 108.284, 24.066. EI MS m/z: 275.7 [$(M+K)^+$] (calcd 276.0); 313.7 [$(M-H+2K)^+$] (calcd 314).

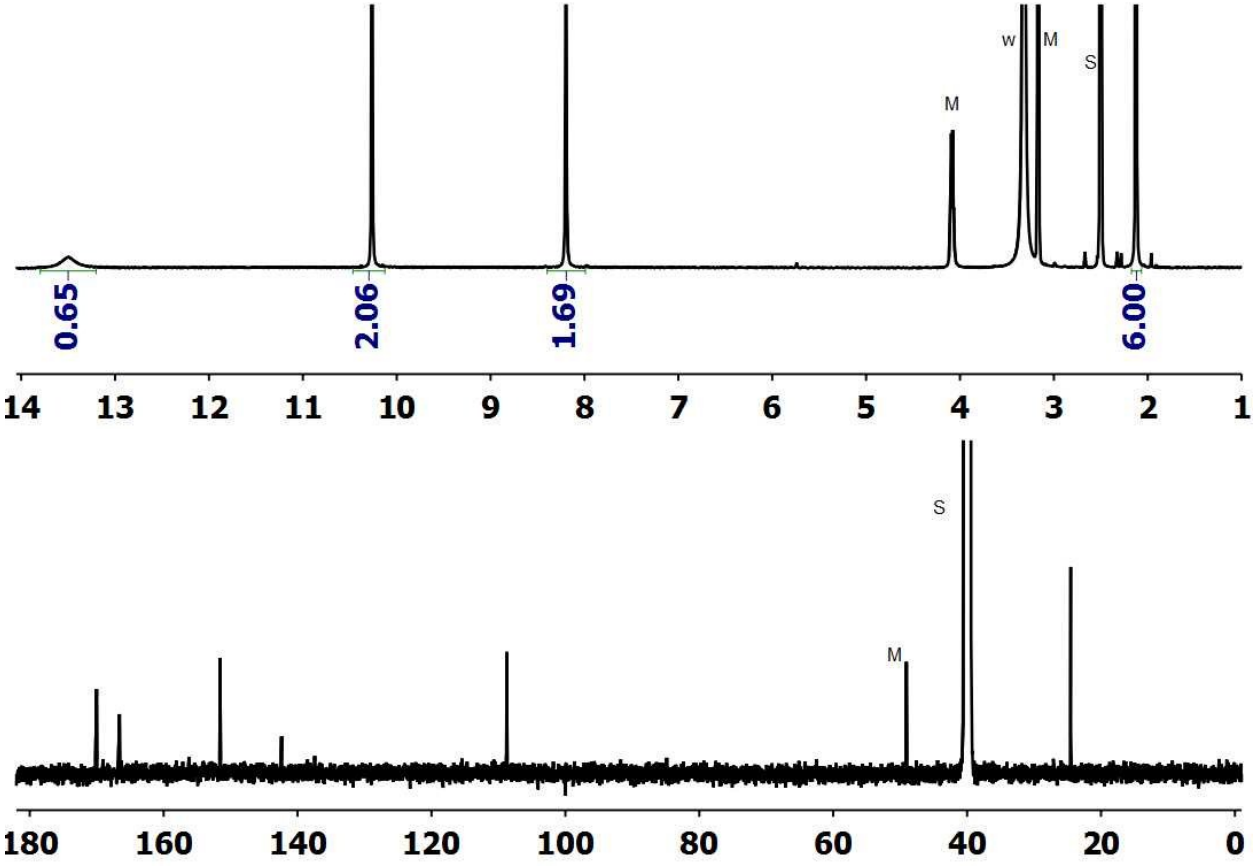

Figure SI-1G. ^{1}H (top) and ^{13}C NMR spectra of 2,6-di(acylamino)-4-carboxypyridine (**DAP**) recorded in dmso-d_6. The residual solvents peaks are marked with M (methanol), W (water), and S (dmso).

S3B. Preparation of **SALI-F3G** and **SALI-DAP**

Preparation and characterization of **SALI-F3G** and **SALI-DAP** were achieved following our published procedure.[4] In brief, a 45 mg portion of activated pristine **NU-1000** (0.021 mmol) was loaded into a 10 mL vial (VWR). Subsequently, a 7 mL of a 0.03 M solution of **F3G-H** or **DAP-H** (0.21 mmol) in a mixture of 2:3 DMSO:MeCN solvent was added to the reaction vial, which was then capped and heated at 60 °C for 24 h with occasional swirling. The supernatant of the reaction mixture was decanted and the MOF sample was soaked in fresh DMSO-MeCN solvent, filtered, washed sequentially with acetone and dichloromethane (40 and 30 mL each), and finally dried in a vacuum oven (~100 torr) for 30 min at 50 °C. The ^{1}H NMR of the digested SALI-CFG materials in 10% D_2SO_4/DMSO-d_6 suggests the incorporation of an average 4 **F3G** and ca 2.3 **DAP** units per Zr_6 node.

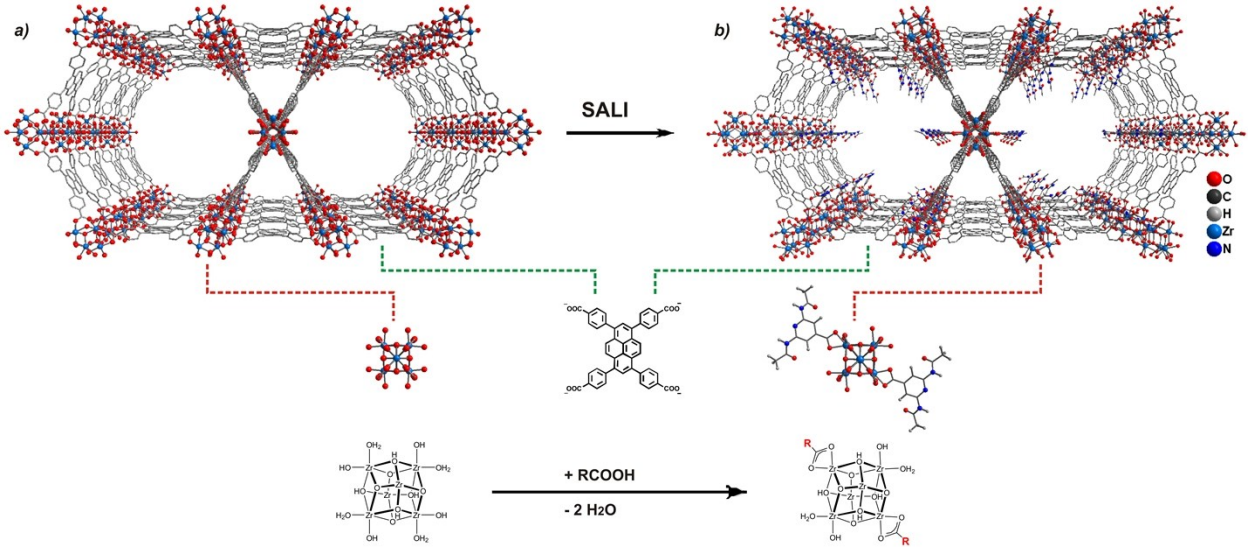

Figure SI-2. Schematic diagram showing functionalization of (a) **NU-1000** in synthesis of (b) **SALI-DAP** *via* SALI.

S3C. Characterization of **SALI-F3G** and **SALI-DAP**

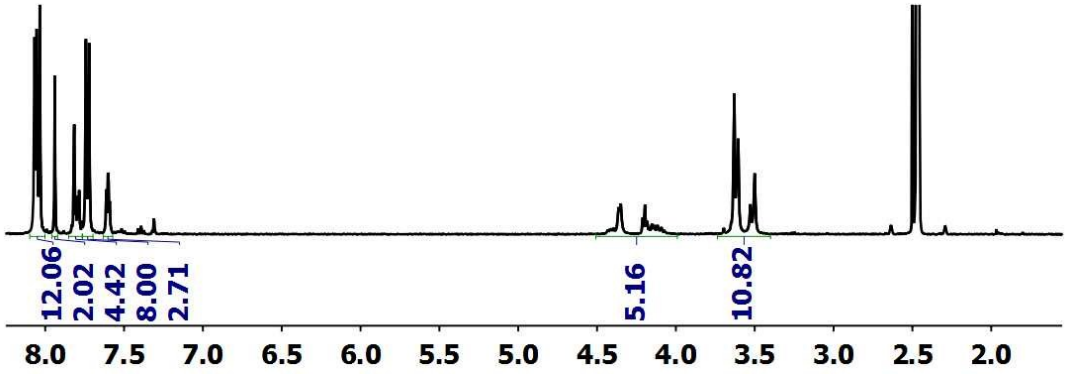

Figure SI-3. ^{1}H NMR spectra of **SALI-F3G** after digesting in 10% D_2SO_4/DMSO-d_6.

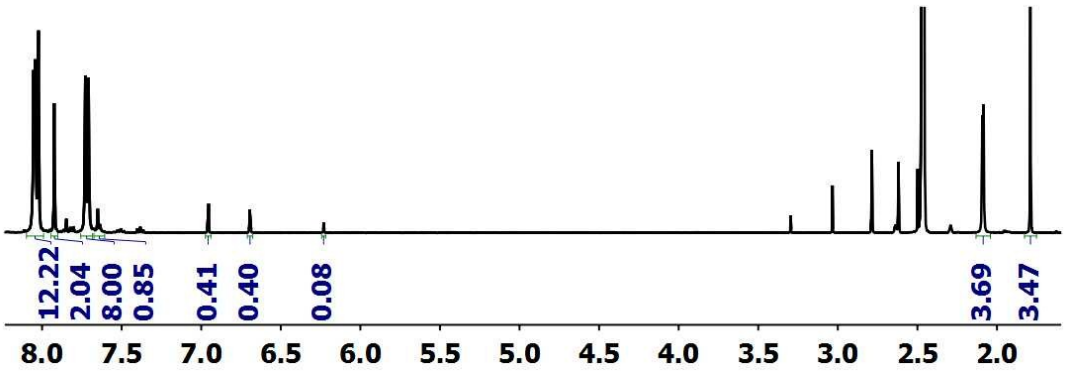

Figure SI-4. ^{1}H NMR spectra of **SALI-DAP** after digesting in 10% D_2SO_4/DMSO-d_6. Note that the total peak intensity (relative to that of H_4TBAPy) of the two methyl groups was used for estimating the degree of DAP incorporation in the NU-1000 cavities, as it decomposes under strong acidic condition (D_2SO_4).

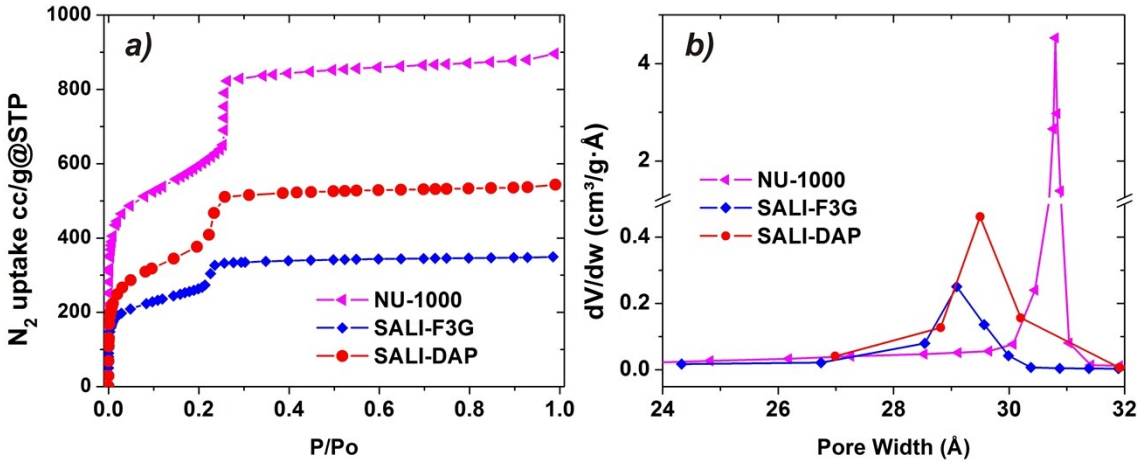

Figure SI-5. (a) N_2 adsorption isotherms at 77 K for **NU-1000**, **SALI-F3G**, and **SALI-DAP** samples and (b) their corresponding BJH pore size distributions calculated from the desorption branch of the N_2 isotherms.

Table SI-1. BET surface area, pore volume and pore diameter of NU-1000 and SALI-derived materials.

MOF	Ligand	BET Surface Area (m^2 g^{-1})	Pore Volume (cc g^{-1})	BJH pore diameter (Å)
NU-1000	-OH, -OH_2	2145	1.46	31
SALI-DAP	DAP (2/node)	1225	0.84	29.5
SALI-F3G	F3G (4/node)	890	0.54	29

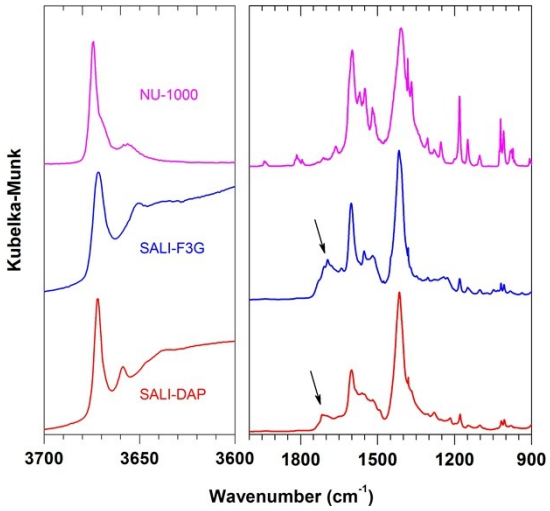

Figure SI-6. DRIFTS plot of **NU-1000**, **SALI-F3G**, and **SALI-DAP** samples. The arrows in the right panel denote the signature of the amide bond in F3G and DAP units.

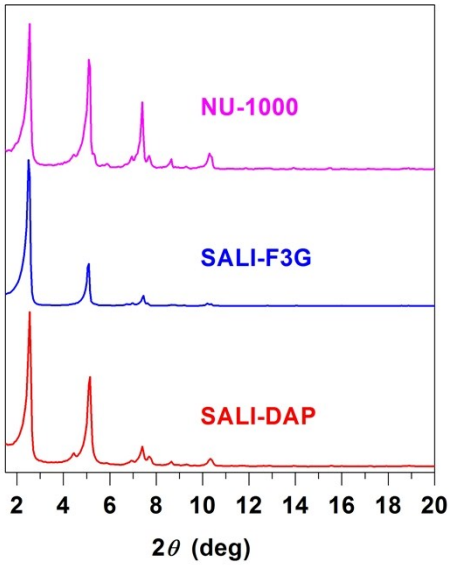

Figure SI-7. PXRD patterns of **NU-1000**, **SALI-F3G**, and **SALI-DAP** samples.

S4. Volumetric Experimental Isotherms for NU-1000 and SALI-derived Materials

Volumetric CO_2 and N_2 isotherms were calculated from the gravimetric isotherms by using the carboxylic acid loading, determined by ^1H NMR shown in Table SI-1 (Section S3C). Binding of each R-COO moiety to each of the four equatorial Zr^{IV} of the Zr_6 nodes entails the removal of two water molecules.[3, 4, 11] Using the crystallographically predicted density for **NU-1000** (0.49 g/cc) and based on simple molecular formula calculations, we estimated densities of **SALI-F3G** and **SALI-DAP** to be 0.83 g/cc and 0.58 g/cc, respectively.

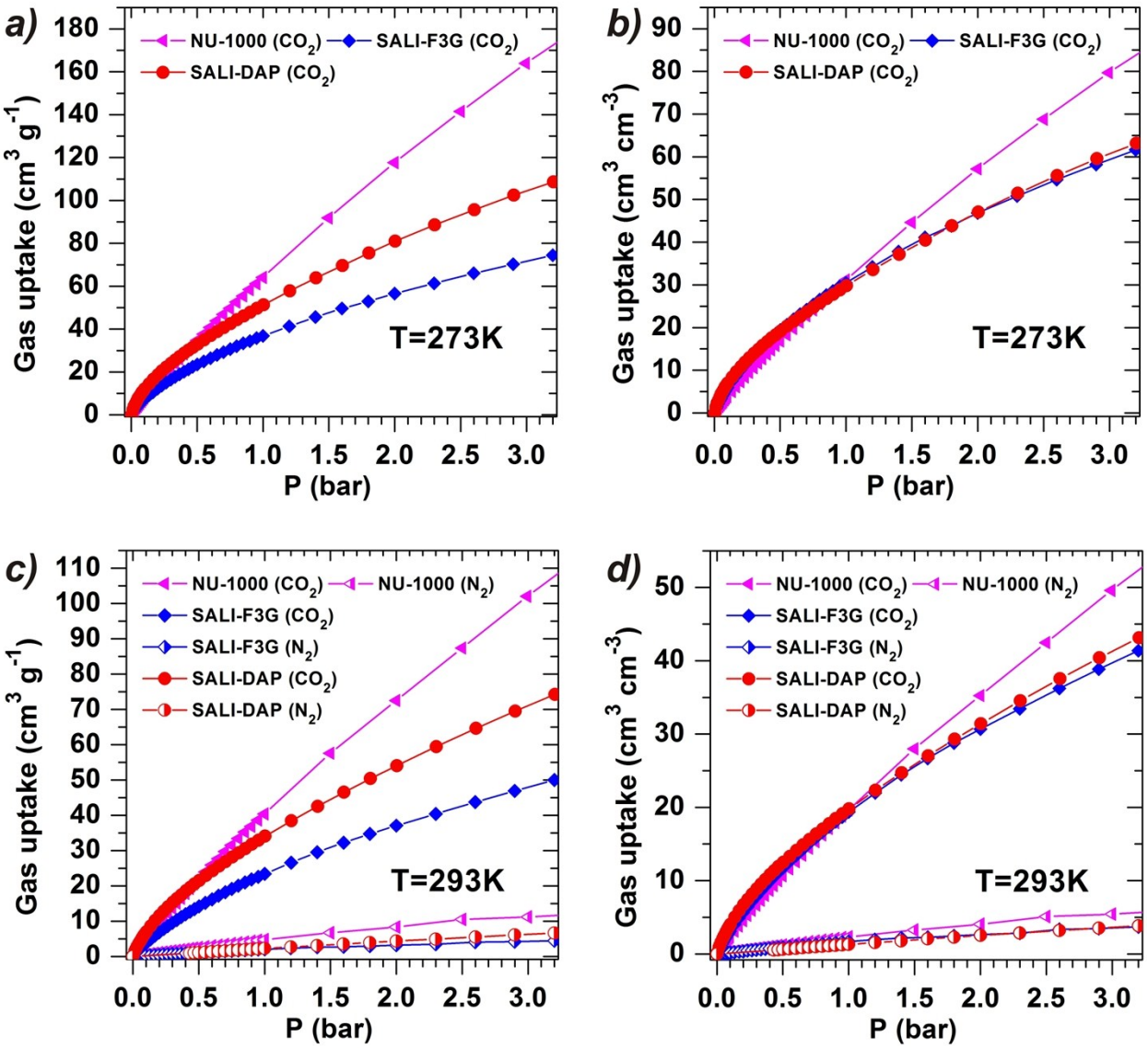

Figure SI-8. Gravimetric (a, c) and volumetric (b, d) isotherms for **NU-1000**, **SALI-F3G**, and **SALI-DAP** samples recorded at 273 K and 293 K, respectively.

S5. Q_{st} Analysis of the Experimental Isotherms

The CO_2 isotherms for **NU-1000**,[4] **SALI-F3G** and **SALI-DAP** samples show Langmuir type behavior. Multi-temperature gravimetric isotherms were collected for these samples at 273-303 K and they were subsequently fit with the dual site Langmuir model:

$$N = \frac{n_1^{sat} b_1 P}{(1 + b_1 P)} + \frac{n_2^{sat} b_2 P}{(1 + b_2 P)}$$

where N is the total gravimetric uptake of CO_2 (mmol/g) at pressure P; n_i^{sat} and b_i are the saturation loading and Langmuir affinity parameter for site i, respectively.

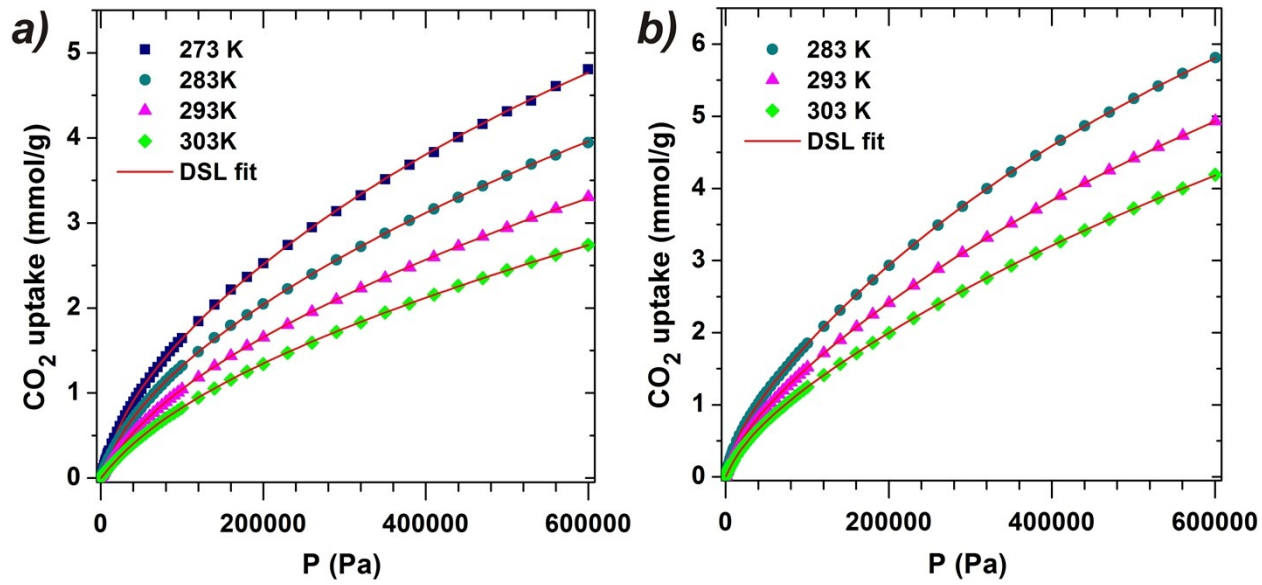

Figure SI-9. Dual site Langmuir (DSL) fits for experimental CO_2 adsorption isotherms at 273-303 K for (a) **SALI-F3G** and (b) **SALI-DAP** samples. R^2_{fit} = 0.9999

Table SI-2. DSL fitting parameters.

MOF	Ads. Site	Param.	273 K	283 K	293 K	303 K	Qst^0 (kJ/mol)
SALI-F3G	Site 1	n^{sat}_1 (mmol g^{-1})	1.01(0.02)	1.01(0.02)	1.01(0.02)	1.01(0.02)	28(1)
		b_1 (Pa^{-1})	3.0(0.06)E-5	2.0(0.05)E-5	1.0(0.03)E-5	0.8(0.02)E-5	
	Site 2	n^{sat}_2 (mmol g^{-1})	10.93(0.15)	10.93(0.15)	10.93(0.15)	10.93(0.15)	
		b_2 (Pa^{-1})	8.9(0.2)E-7	6.4(0.2)E-7	4.7(0.1)E-7	3.5(0.0)E-7	
SALI-DAP	Site 1	n^{sat}_1 (mmol g^{-1})	-	0.65(0.01)	0.65(0.01)	0.65(0.01)	27(1)
		b_1 (Pa^{-1})	-	7.0(0.5)E-5	5.0(0.06)E-5	3.0(0.04)E-5	
	Site 2	n^{sat}_2 (mmol g^{-1})	-	13.29(0.05)	13.29(0.05)	13.29(0.05)	
		b_2 (Pa^{-1})	-	1.06(0.01)E-7	0.80(0.01)E-7	0.61(0.01)E-7	

The errors in the parameters are listed in the parenthesis.

These DSL fitting parameters were used to deduce a form where pressure P is expressed as a function of N and then Q_{st} values were calculated using the Clausius-Clapeyron equation:

$$(lnP)_N = -\frac{Q_{st}}{RT} + Const$$

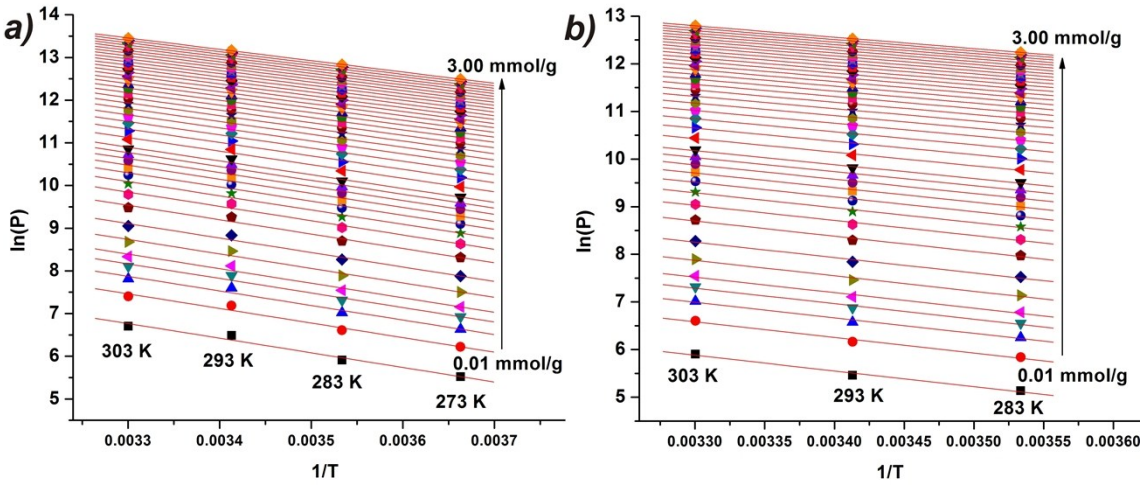

Figure SI-10. CO_2 adsorption isosteres for (a) **SALI-F3G** and (b) **SALI-DAP** samples.

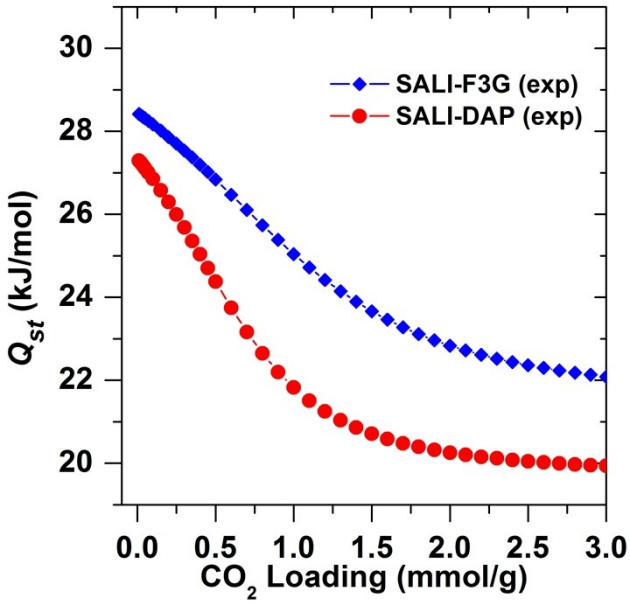

Figure SI-11. Q_{st} plots calculated from experimental isotherm data for **SALI-F3G** and **SALI-DAP**.

S6. Details of the Molecular Simulations

S6A. Binding energy calculation by *ab initio* method

The CO_2 binding energies with the individual **F3G-H** and **DAP-H** functional groups were calculated using the Gaussian09[12] software. The geometry optimizations were implemented at the B3LYP level of density functional theory using a 6-311+G(d, p) basis set. Energy minimizations were started at several different positions of CO_2 around the functional group to locate the lowest potential energy minimum. Single-point energy calculations, followed by frequency calculations, were carried out for the lowest energy structures using MP2 calculations

with a 6-311+G(d,p) basis set. To compensate for basis set superposition errors, the obtained binding energies were corrected by the counterpoise method.[13] Atomic partial charges of free, **F3G-H**-bound, and **DAP-H**-bound CO_2 molecules were obtained using the ChelpG method at the MP2 level.

S6B. Geometry optimization of MOFs

Atomic coordinates for the parent framework **NU-1000** were obtained from previous work,[2] with the modification to the protonation state of the zirconium nodes that has been recently determined via electronic structure calculations by Planas et al.;[14] the final structure has four aqua and four hydroxyl ligands per zirconium node. From this starting **NU-1000** structure, we generated **SALI-F3G** and **SALI-DAP** structures by manual modification of the framework: one aqua and one hydroxyl ligand per equatorial Zr(IV) of the Zr_6 node were replaced by a carboxylate based ligand. For **SALI-F3G**, each Zr_6 node was functionalized with four F3Gs (see Figure SI-12); whereas in **SALI-DAP**, each metal node was functionalized with two DAPs, to be consistent with the experimental data (^{1}H NMR). The resulting structures were optimized with the Forcite module of Materials Studio[15] using the Smart algorithm that is a cascade of the steepest descent, adjusted basis set Newton-Raphson (ABNR) and quasi-Newton methods. Bonded and non-bonded interactions were treated using the Universal Force Field (UFF).[16] The partial charges for the parent framework were derived from the extended charge equilibration method (EQeq),[17] and the atomic charges for the F3G and DAP groups were taken from OPLS[18] and CHARMM22,[19] respectively. A cutoff distance of 12.8 Å was used for the Lennard-Jones interactions. The long-range electrostatic interactions arising from the presence of partial atomic charges were calculated by the Ewald method.

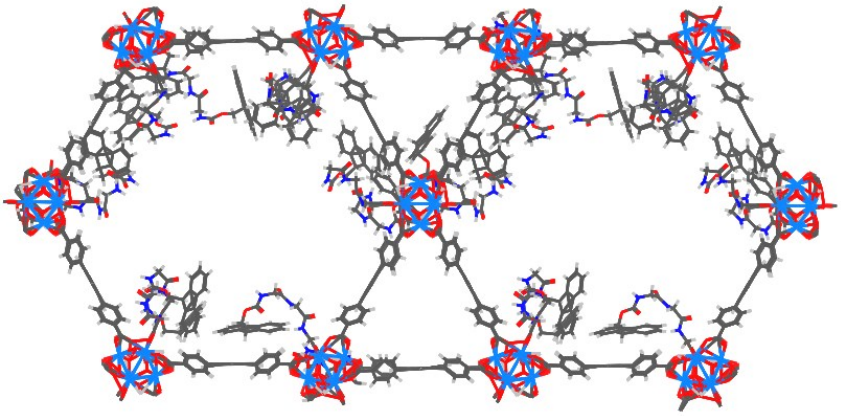

Figure SI-12. Molecular representation of **SALI-F3G** (along the c-axis).

S6C. GCMC simulation

The adsorption of CO_2 and N_2 were investigated using grand canonical Monte Carlo (GCMC) simulations performed with our in-house code RASPA.[20] We used atomistic models for **NU-1000**, **SALI-F3G**, and **SALI-DAP** MOF structures, generated as described above. **NU-1000** and **SALI-DAP** were treated as rigid frameworks. Since F3G is flexible, **SALI-F3G** was relaxed at 273 K by molecular dynamics (MD) simulation for 1 ns, and the final structure was used (held rigid) for the subsequent GCMC simulations. Standard Lennard-Jones (LJ) + Coulomb potentials were used to model the interactions between the framework and gas atoms. The Lennard-Jones parameters for the framework atoms were taken from the UFF force field. For the functional

groups F3G and DAP, the OPLS[18] and CHARMM22[19] force fields, respectively, were used to describe the bonded and non-bonded interactions. Partial atomic charges for the **NU-1000** framework atoms were derived from the extended charge equilibration method (EQeq),[17] and the charges for the F3G and DAP groups were taken from OPLS[18] and CHARMM22,[19] respectively. The Lorentz-Berthelot mixing rules were employed to calculate gas/solid LJ parameters, and LJ interactions beyond 12.8 Å were neglected. The Ewald sum method was used to compute the electrostatic interactions. CO_2 and N_2 were modeled using the TraPPE potential with Lennard-Jones + Coulomb interactions.[21] At least 6×10^4 Monte Carlo cycles were performed, the first 50% of which were used for equilibration, and the remaining cycles were used to calculate the ensemble averages. In each cycle, insertion, deletion, translation and rotation moves were performed with equal probability.

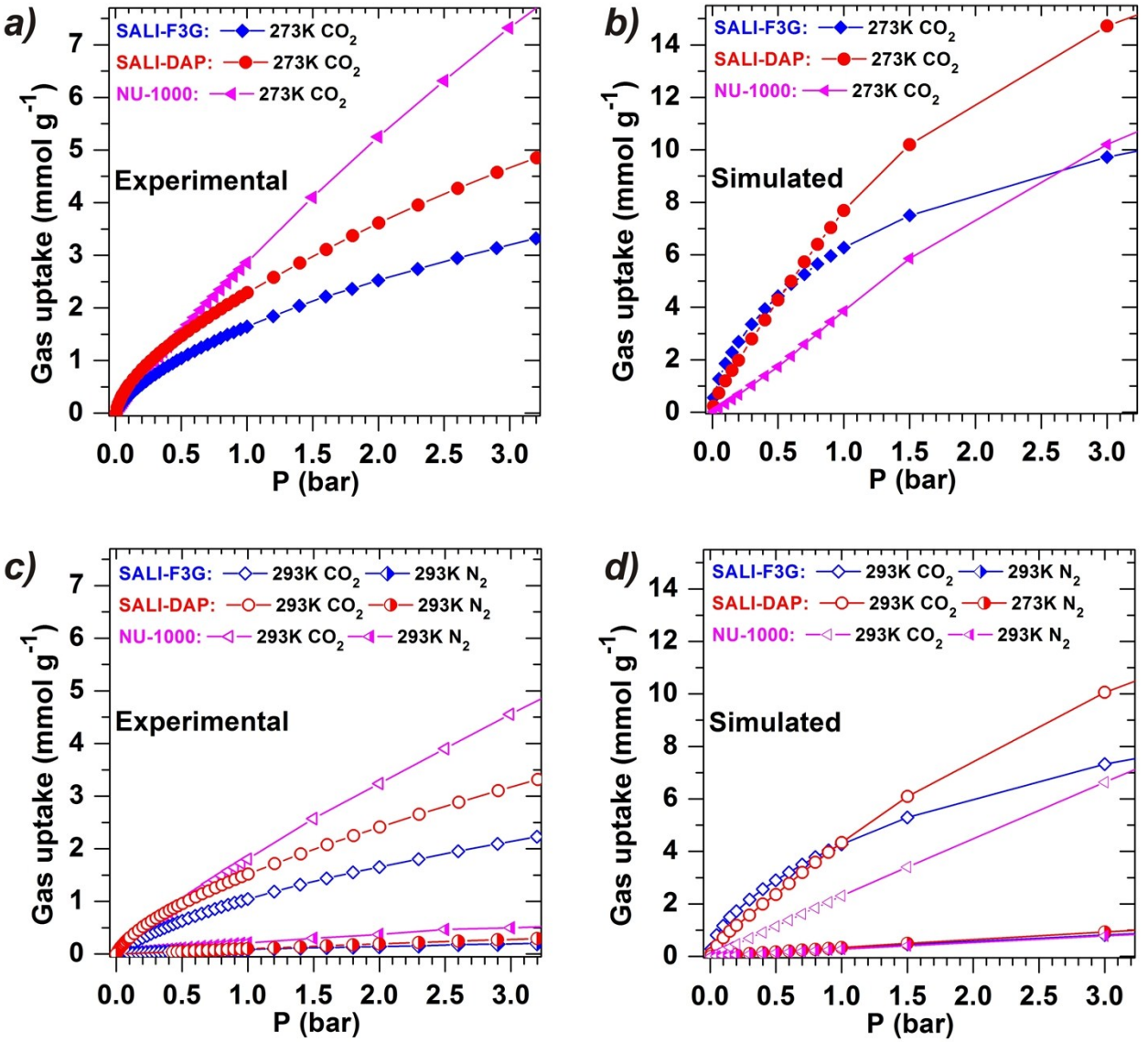

Figure S13. Comparison of (a, c) experimental CO_2 and N_2 isotherms with those obtained *via* (b, d) GCMC simulation at two different temperatures for **SALI-F3G** (blue diamond), **SALI-DAP** (red circle), and **NU-1000** (purple triangle). Note that (1) N_2 isotherms were compared only at 293 K and (2) while the GCMC simulations

overestimate the total uptake, the trends for **SALI-F3G** versus **SALI-DAP** are in qualitative agreement with the experimental data presented in panel a.

To test the influence of the flexibility of **F3G** on the CO_2 adsorption behavior in **SALI-F3G**, a hybrid MC/MD simulation in the NVE ensemble was performed. Each cycle consisted of 5 MD steps (1 fs time step) used as a hybrid MC move plus the usual GCMC moves. The OPLS force field parameters mentioned above for bond bending, bond stretching and torsional potentials were used for the flexible F3G groups. As shown in Figure S14, a similar CO_2 isotherm and heat of adsorption were observed for **SALI-F3G** with rigid and flexible functional groups.

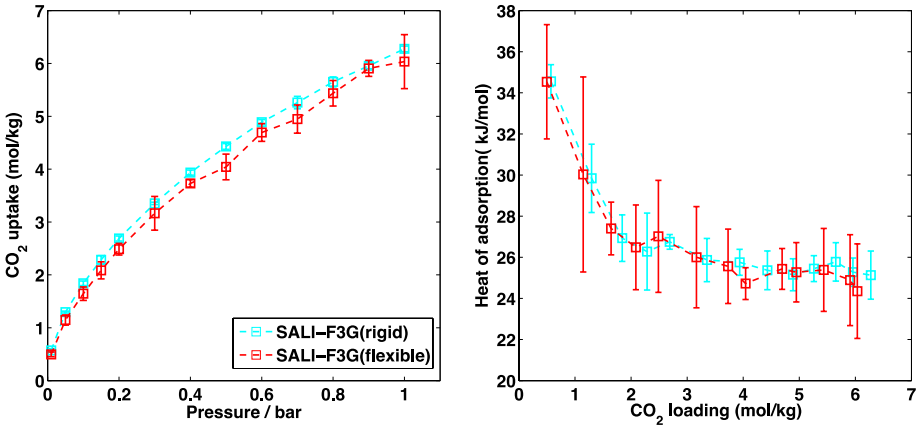

Figure S14. Comparison of CO_2 isotherm at 273 K (a) and heat of adsorption (b) for **SALI-F3G** with rigid and flexible F3G.

Table SI-3 Comparison of binding properties of CO_2 from DFT in this work with literature

	∠O-C-O (°)	D···C (CO_2) (Å)	D···O (CO_2) (Å)	C=O (CO_2) (Å)
CO_2 (DFT)	180			1.16
CO_2-F3G-H (DFT)	177.95	2.94	2.35	1.16
CO_2-DAP-H (DFT)	178.64	3.19	2.26	1.16
CO_2-Fe_2(dobc) (exp)[22]	179	2.29	2.29	–
CO_2-$Zn_2(Atz)_2$(ox) (exp)[23]	175.72	3.152	–	1.108

D: the interacting atom at the primary binding site in MOFs.

The O-C-O angle in the **F3G-H** and **DAP-H** bound CO_2 is close to the experimentally measured data in CO_2-Fe_2(dobc) and slightly higher (i.e. more linear) compared to that in CO_2-$Zn_2(Atz)_2$(ox). In the Fe_2(dobc) system, the Lewis acidic (coordinatively unsaturated) metal site strongly binds CO_2 via one of its oxygen atoms manifesting a shorter M-O[CO] distance (2.29 Å)[22] compared to those observed for the CO_2 bound in organic COMs. On the contrary, the Lewis basic amine group reported in $Zn_2(Atz)_2$(ox) manifests N-C[O_2] distance (3.152 Å)[23] close

to that computed for the COMs (F3G-H and DAP-H). Furthermore, our DFT computations reveal that the C=O bond length remains unchanged upon binding with the COM; this finding is in line with the distribution of the partial charges of bound CO_2 (Figure S15), which change only insignificantly compared to a gas-phase CO_2 molecule.

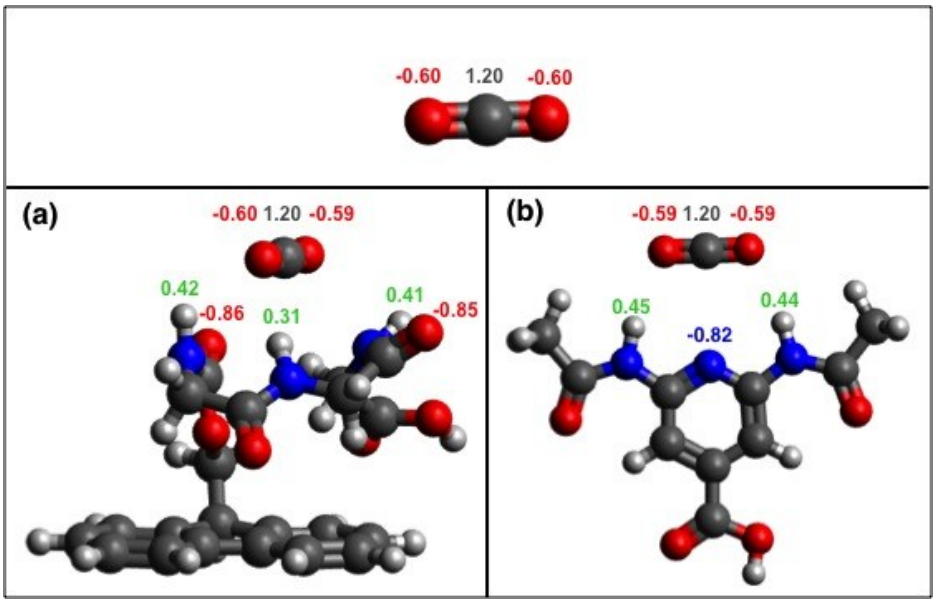

Figure SI-15. Atomic partial charges for free CO_2, **F3G**-bound CO_2 (a), and **DAP**-bound CO_2 (b).

S7. Control experiments with non-COM functional groups

To justify whether the improved Q_{st} values in **SALI-DAP** and **SALI-F3G** are indeed mainly due to selective binding of CO_2 in these COMs, we designed two control samples that does not bear any COM or COM-forming functionality. We prepared FMoc-protected dialanine peptide (*i.e.* **F2A-H**) and *o*-aminobenzoic acid (*i.e.* **OAB-H**) functionalized **NU-1000** samples (Scheme SI-2). The ^{1}H NMR data of the resulting materials (i.e. **SALI-F2A** and **SALI-OAB**; Figure SI-16) show similar degree of node functionalization (i.e. 3-4/node), and the N_2 isotherms (77 K; Figure SI-17) reveal comparable pore dimension and/or volume relative to **SALI-F3G** and **SALI-DAP** samples. Recall that **F3G-H** was chosen for its torsional flexibility due to the absence of side chains in its backbone, which in turn helps it adopt a COM. We reasoned that incorporating a methyl group in the peptide backbone could effectively induce a non-COM or a different conformation relative to the COM conformation adopted by flexible **F3G-H**. The characterization data suggest that **SALI-F2A** and **SALI-OAB** would be good control samples with comparable physical parameters (Table SI-4) to the COM units. Figure SI-18 highlights the corresponding Q_{st} data; as expected, **SALI-F2A** and **SALI-OAB** show lower Q_{st} values at low loading and eventually plateau at ca 22 kJ/mol, which is the Q_{st} of the 'secondary' binding sites in functionalized **NU-1000** due to reduced pores. With these data for two control samples, we can unambiguously discern the conclusion that we made for the COM.

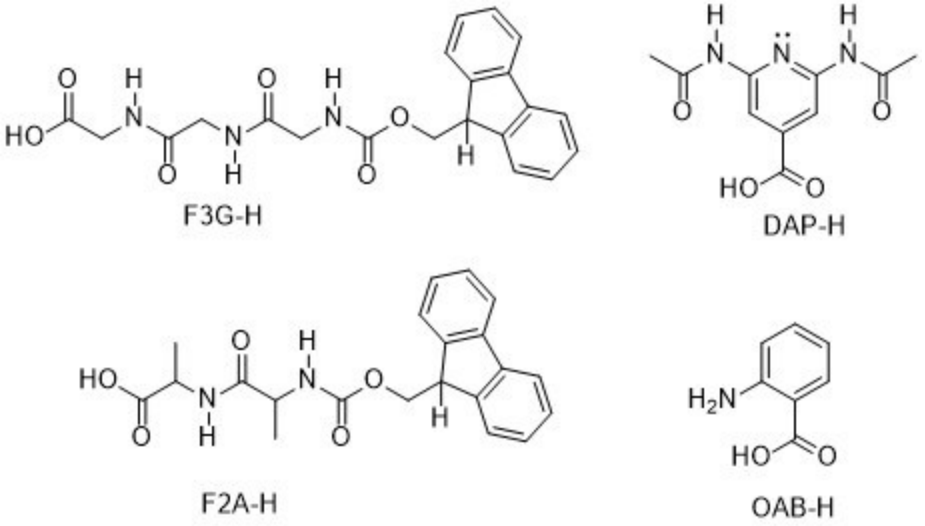

Scheme SI-2. Chemical structures of carboxylate functional groups: (top) COM as **F3G-H** and **DAP-H**; (bottom) non-COM control as **F2A-H** and **OAB-H**.

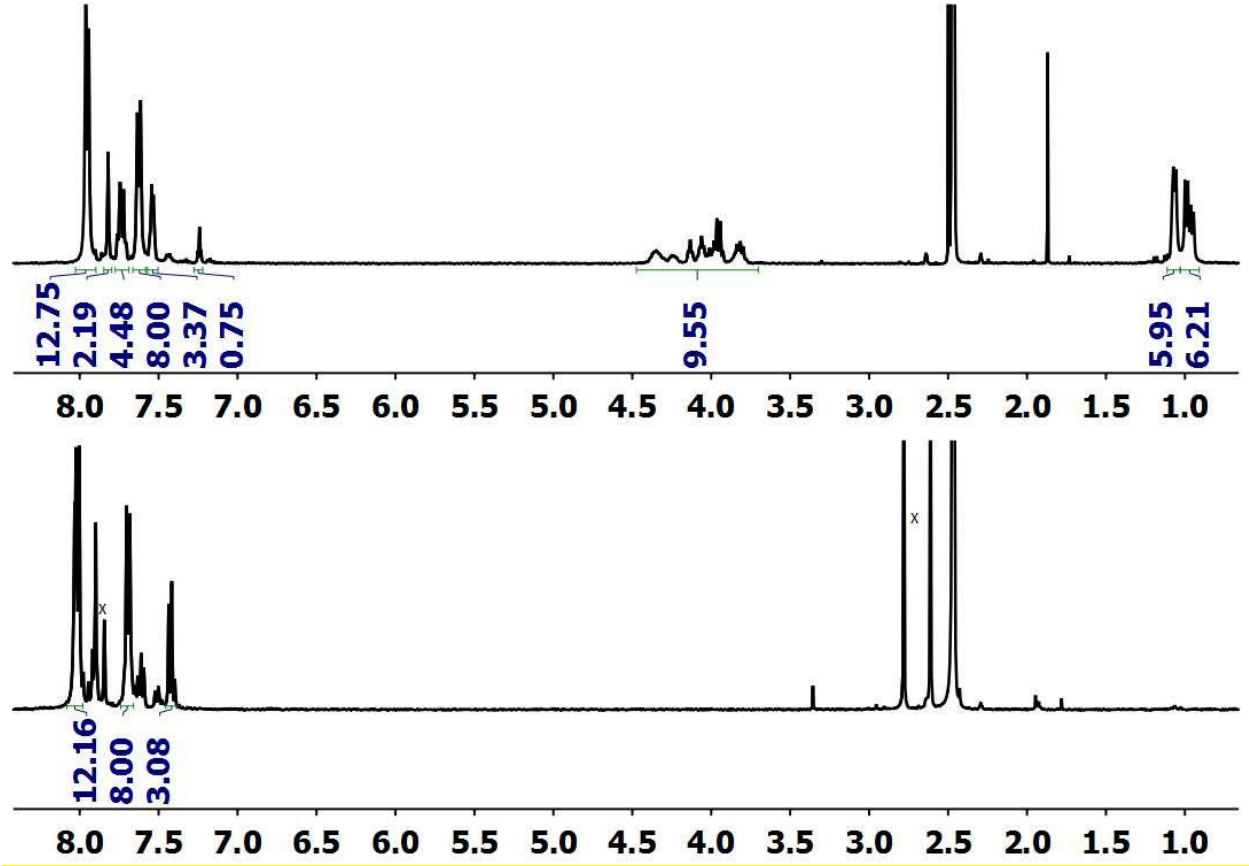

Figure SI-16. ^{1}H NMR spectra of (top) **SALI-F2A** and (bottom) **SALI-OAB** samples after digesting in 10% D_2SO_4/DMSO-d_6.

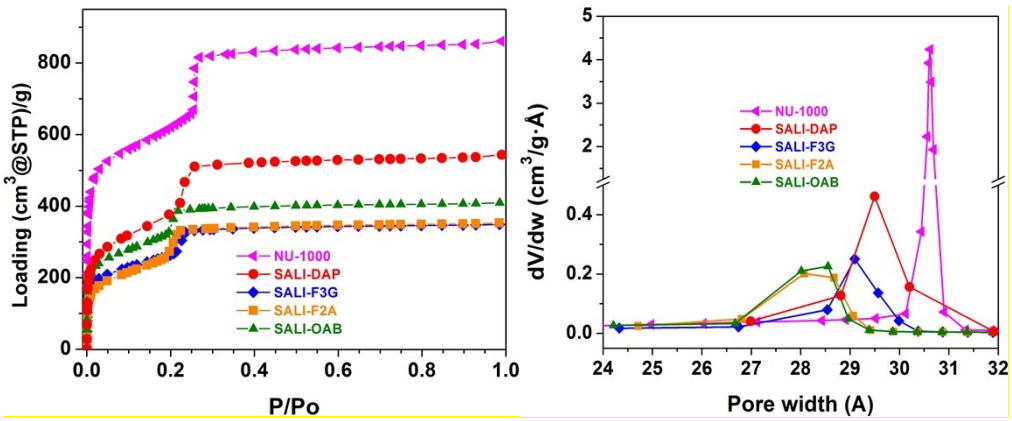

Figure SI-17. (Left) N_2 adsorption isotherms at 77 K for **NU-1000**, and SALI-derived samples and (right) their corresponding BJH pore size distributions calculated from the desorption branch of the N_2 isotherms.

Table SI-4. BET surface area, pore volume and pore diameter of NU-1000 and SALI-derived materials.

MOF	Ligand	BET Surface Area (m^2 g^{-1})	Pore Volume (cc g^{-1})	BJH pore diameter (Å)
NU-1000	-OH, -OH_2	2145	1.46	31
SALI-DAP	DAP (2/node)	1225	0.84	29.5
SALI-F3G	F3G (4/node)	890	0.54	29
SALI-F2A	F2A (4/node)	850	0.54	28.6
SALI-OAB	OAB (3/node)	1080	0.63	28.7

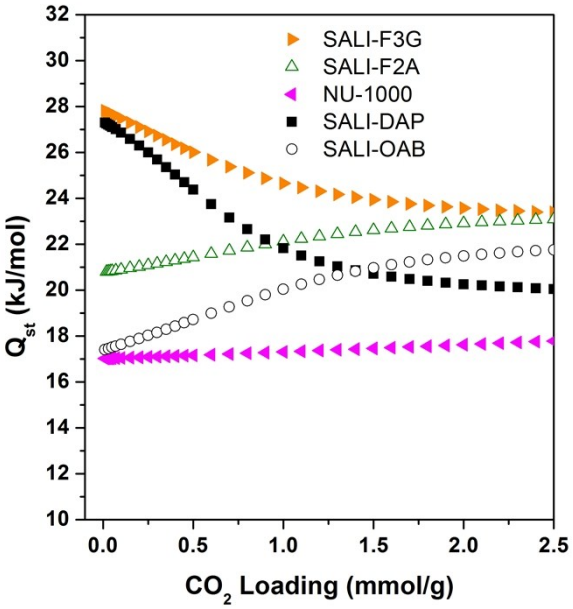

Figure SI-18. Q_{st} plots calculated from experimental isotherm data for **NU-1000**, and SALI-derived samples.

Table SI-5. Gravimetric working capacity of NU-1000 and SALI-derived materials at PSA and VSA conditions for flue gas CO_2 (PSA: between 0.9 bar and 0.15 bar, VSA: between 0.225 bar and 0.0075 bar) obtained from the 293 K CO_2 adsorption isotherms.[24]

MOF	Under flue-gas CO_2 condition	
	PSA (mmol g^{-1})	VSA (mmol g^{-1})
NU-1000	1.33	0.45
SALI-DAP	1.01	0.53
SALI-F3G	0.73	0.33

References

1. K. C. Stylianou, R. Heck, S. Y. Chong, J. Bacsa, J. T. A. Jones, Y. Z. Khimyak, D. Bradshaw and M. J. Rosseinsky, *J. Am. Chem. Soc.*, 2010, **132**, 4119-4130.
2. J. E. Mondloch, W. Bury, D. Fairen-Jimenez, S. Kwon, E. J. DeMarco, M. H. Weston, A. A. Sarjeant, S. T. Nguyen, P. C. Stair, R. Q. Snurr, O. K. Farha and J. T. Hupp, *J. Am. Chem. Soc.*, 2013, **135**, 10294-10297.
3. P. Deria, W. Bury, J. T. Hupp and O. K. Farha, *Chem. Commun.*, 2014, **50**, 1965-1968.
4. P. Deria, J. E. Mondloch, E. Tylianakis, P. Ghosh, W. Bury, R. Q. Snurr, J. T. Hupp and O. K. Farha, *J. Am. Chem. Soc.*, 2013, **135**, 16801-16804.
5. J. Rouquerol, P. Llewellyn and F. Rouquerol, *Stud. Surf. Sci. Catal.*, 2007, **160**, 49-56.
6. K. S. Walton and R. Q. Snurr, *J. Am. Chem. Soc.*, 2007, **129**, 8552-8556.
7. M. Kruk, M. Jaroniec and A. Sayari, *Langmuir*, 1997, **13**, 6267-6273.
8. A. Llanes-Pallas, C.-A. Palma, L. Piot, A. Belbakra, A. Listorti, M. Prato, P. Samorì, N. Armaroli and D. Bonifazi, *J. Am. Chem. Soc.*, 2009, **131**, 509-520.
9. M. Nettekoven and C. Jenny, *Org. Process Res. Dev.*, 2003, **7**, 38-43.
10. T. Ueda, H. Konishi and K. Manabe, *Org. Lett.*, 2013, **15**, 5370-5373.
11. P. Deria, J. E. Mondloch, O. Karagiaridi, W. Bury, O. K. Farha and J. T. Hupp, *Chem. Soc. Rev.*, 2014, **43**, 5896-5912.
12. M. J. Frisch, G. W. Trucks, H. B. Schlegel, G. E. Scuseria, M. A. Robb, J. R. Cheeseman, G. Scalmani, V. Barone, B. Mennucci, G. A. Petersson, H. Nakatsuji, M. Caricato, X. Li, H. P. Hratchian, A. F. Izmaylov, J. Bloino, G. Zheng, J. L. Sonnenberg, M. Hada, M. Ehara, K. Toyota, R. Fukuda, J. Hasegawa, M. Ishida, T. Nakajima, Y. Honda, O. Kitao, H. Nakai, T. Vreven, J. A. Montgomery, Jr., J. E. Peralta, F. Ogliaro, M. Bearpark, J. J. Heyd, E. Brothers, K. N. Kudin, V. N. Staroverov, R. Kobayashi, J. Normand, K. Raghavachari, A. Rendell, J. C. Burant, S. S. Iyengar, J. Tomasi, M. Cossi, N. Rega, M. J. Millam, M. Klene, J. E. Knox, J. B. Cross, V. Bakken, C. Adamo, J. Jaramillo, R. Gomperts, R. E. Stratmann, O. Yazyev, A. J. Austin, R. Cammi, C. Pomelli, J. W. Ochterski, R. L. Martin, K. Morokuma, V. G. Zakrzewski, G. A. Voth, P. Salvador, J. J. Dannenberg, S. Dapprich, A. D. Daniels, Ö. Farkas, J. B. Foresman, J. V. Ortiz, J. Cioslowski and D. J. Fox, *Gaussian 09*, Revision D.01. Gaussian Inc., Wallingford CT, 2009

13. S. F. Boys and F. Bernardi, *Mol. Phys.*, 1970, **19**, 553-566.
14. N. Planas, J. E. Mondloch, S. Tussupbayev, J. Borycz, C. J. Cramer, J. T. Hupp, O. K. Farha and L. Gagliardi, *J. Phys Chem. Lett.*, 2014, **5**, 3716-3723.
15. *Materials Studio 5.0*, Accelrys Software Inc., San Diego, CA 92121, USA
16. A. K. Rappé, C. J. Casewit, K. S. Colwell, W. A. Goddard and W. M. Skiff, *J. Am. Chem. Soc.*, 1992, **114**, 10024.
17. C. E. Wilmer, K. C. Kim and R. Q. Snurr, *J. Phys. Chem. Lett.*, 2012, **3**, 2506-2511.
18. X. Mu, K. M. Eckes, M. M. Nguyen, L. J. Suggs and P. Ren, *Biomacromolecules*, 2012, **13**, 3562-3571.
19. A. D. MacKerell, D. Bashford, M. Bellott, R. L. Dunbrack, J. D. Evanseck, M. J. Field, S. Fischer, J. Gao, H. Guo, S. Ha, D. Joseph-McCarthy, K. K. L. Kuchnir, F. T. K. Lau, C. Mattos, S. Michnick, T. Ngo, D. T. Nguyen, B. Prodhom, W. E. Reiher, B. Roux, M. Schlenkrich, J. C. Smith, R. Stote, J. Straub, M. Watanabe, J. Wirkiewicz-Kuczera, D. Yin and M. Karplus, *J. Phys. Chem. B*, 1998, **102**, 3586-3616.
20. D. Dubbeldam, S. Calero, D. E. Ellis and R. Q. Snurr, *Mol. Simul.*, 2015, DOI: 10.1080/08927022.08922015.01010082.
21. J. J. Potoff and J. I. Siepmann, *AlChE J.*, 2001, **47**, 1676.
22. W. L. Queen, M. R. Hudson, E. D. Bloch, J. A. Mason, M. I. Gonzalez, J. S. Lee, D. Gygi, J. D. Howe, K. Lee, T. A. Darwish, M. James, V. K. Peterson, S. J. Teat, B. Smit, J. B. Neaton, J. R. Long and C. M. Brown, *Chem. Sci.*, 2014, **5**, 4569-4581.
23. R. Vaidhyanathan, S. S. Iremonger, G. K. H. Shimizu, P. G. Boyd, S. Alavi and T. K. Woo, *Science*, 2010, **330**, 650-653.
24. G. Srinivas, V. Krungleviciute, Z.-X. Guo and T. Yildirim, *Energy Environ. Sci.*, 2014, **7**, 335-342.